Research Article | Vol. 31, No. 3 / 30 Jan 2023 / Optics Express 5102

Optics EXPRESS

Fast all-fiber ultraviolet photodetector based on an Ag-decorated ZnO micro-pillar

DINGBANG MA,[1,2] YING WANG,[1,2,*] CHEN CHEN,[1,2] ZHIHAO CAI,[1,2] JIAXIONG ZHANG,[1,2] CHANGRUI LIAO,[1,2] XIAOYU WENG,[1] LIWEI LIU,[1] JUNLE QU,[1] AND YIPING WANG[1,2]

[1]*Key Laboratory of Optoelectronic Devices and Systems of Ministry of Education/GuangDong Province, College of Physics and Optoelectronic Engineering, Shenzhen University, Shenzhen 518060, China*
[2]*Shenzhen Key Laboratory of Photonic Devices and Sensing Systems for Internet of Things, Guangdong and Hong Kong Joint Research Centre for Optical Fibre Sensors, Shenzhen University, Shenzhen 518060, China*
[*]*yingwang@szu.edu.cn*

Abstract: There are urgent demands of ultraviolet (UV) photodetectors with high sensitivity and fast response due to the wide application of ultraviolet light in the fields of medical treatment, space exploration, optical communication and semiconductor industry. The response speed of traditional ZnO-based UV photodetectors is always limited by the carrier mobility and electrical resistance caused by the external circuits. Utilizing the all-optical detection method may replace the complex circuit structure and effectively improve the response speed of photodetectors. Here, a fast-response fiber-optic UV photodetector is proposed, where a ZnO micro-pillar is fixed on the end face of a fiber-tip and acts as a Fabry-Pérot interferometer (FPI). Under the irradiation of UV light, the photo-generated carriers change the refractive index of the ZnO micro-pillar, leading to a redshift of the interference wavelengths of the ZnO FPI. To enhance this effect, a discontinuous Ag film with an island-like structure is coated on the surface of ZnO micro-pillars through magnetron sputtering, and therefore the sensitivity of the proposed device achieves to 1.13 nm/(W·cm^{-2}), which is 3.9 times higher than that of without Ag-decoration, due to the intensification of photo-carrier change with the help of the Schottky junction formed between Ag film and ZnO micro-pillar. Meanwhile, since the response speed of the proposed device is mainly determined by the temporal RI change of ZnO micro-pillar, the fiber-optic UV photodetector also shows very fast response with a rise time of 35 ns and a decay time of 40 µs. The demonstrated structure takes full advantage of optical fiber devices, exhibiting compactness, flexibility, fast response and immune to electromagnetic interference, which paves a new way for the next generation of photodetection devices.

1. Introduction

Due to the increasingly wide application of ultraviolet (UV) light in medical health [1], space detection [2], optical communication [3], semiconductor industry [4] and other fields, high-performance UV photodetector (PD) based on different wide bandgap semiconductor are playing an increasingly significant role in UV detection [5–8]. In order to meet the needs of device miniaturization and high sensitivity, UV PDs based on nano-materials have been investigated extensively [9,10]. Zinc oxide (ZnO) is a kind of wide bandgap (≈3.37 eV) semiconductor with large exciton binding energy (≈60 meV), high transparency and excellent UV absorption, so it has become one of the most ideal materials for UV detection [11,12]. In addition, ZnO nanomaterials may significantly shorten the carrier transport time and result in significant photoconductivity gain due to its intrinsic small-sized active region and large specific surface area [13,14]. Yang and his colleagues used ZnO single nanowires for UV detectors in 2002 and obtained excellent UV response [15], which caused an upsurge in the use of ZnO nanomaterials for UV sensing. Furthermore, metal doping have been proven to significantly improve the UV performance of

#481844 https://doi.org/10.1364/OE.481844
Journal © 2023 Received 25 Nov 2022; revised 6 Jan 2023; accepted 6 Jan 2023; published 27 Jan 2023

Optics EXPRESS

ZnO by abundant studies [16–18]. Yang et al. demonstrated that Ag-doping can modulate the surface states and Schottky barrier of ZnO, which greatly affect the response time of UV [19]. Huang et al. adjusted the width of depletion layer by decorating Ag nanoparticles to enhance the detection performance of Ag-ZnO photodetectors [20]. Rainer et al. obtained UV nanosensors based on a single nanowire of silver-doped ZnO, proving that the sensitivity and response speed of the device was significantly improved through Ag-doping [21]. Here, Ag, as one of the metal elements, not only optimizes the nanomaterial's electronic structure but also improves the sensitivity of UV detection [22,23]. Although the performance of UV PDs based on ZnO nanomaterials has achieved great breakthroughs continuously with the deepening of research, the response speed is intrinsically limited to the physical principle and optoelectronic design of PD devices. At present, most of UV PDs are based on photovoltaic or photoconductive effect [24–27] that requires an external circuit to capture the current gain, which often introduces series resistors and increases the carrier migration time, resulting in a longer response time and increase of power consumption. If only the instantaneous carrier change of the material itself can be used to reflect UV intensities [28,29], the response time of the device can be greatly reduced. PDs constructed by an all-optical approach tend to be much faster than that of traditional circuit architectures because photons travel much faster than carriers. To replace the complex circuit in traditional PDs, all-fiber structure should be a satisfactory scheme since optical fiber is a flexible and stable optical transmission medium that enables the steady transmission of optical signals. Meanwhile, by combining with appropriate materials, fiber optic PDs can be realized with fast response and most of the expected operation wavelengths [27,30,31].

In this paper, we propose an all-fiber UV PD that based on a single Ag-decorated ZnO micro-pillar lying on the end face of a single mode fiber (SMF). A Fabry-Pérot interferometer (FPI) is formed by two parallel sidewalls (both are parallel to the fiber end facet) of the ZnO micro-pillar. Under UV irradiation, the photo-generated carriers accumulate instantly due to the small volume size of the ZnO micro-pillar, which leads to the increase of material refractive index (RI) and thus an interference wavelength redshift (shift to the longer wavelengths) of the FPI. And this effect can be dramatically enhanced through decorating ultra-thin discontinuous Ag-film via simple metal sputtering. With coating discontinuous island-like Ag-film onto the ZnO micro-pillar, the sensitivity of the proposed device can be improved up to 3.9 times higher than that of without Ag-decoration, achieving to 1.13 nm/(W·cm^{-2}). More importantly, the device also shows very fast response, with a rise time of 35 ns and a fall time of 40 μs, which is much better than that of the similar type of devices previously reported [28,29].

2. Operation principle and device fabrication

Figure 1(a) shows the schematic diagram of the proposed fiber-optic UV PD. Broadband near infrared probing light delivered through the SMF fiber core reaches to the ZnO micro-pillar and is reflected back into the fiber core by two sidewalls of ZnO micro-pillar, thus forming a fiber-tip FPI. For clarity, a 2D schematic of the UV sensing area is presented in Fig. 1(b), where one can see more clearly that the Ag-decorated ZnO micro-pillar is lying on the endface of the fiber core and its upper and lower parallel sidewalls act as reflection mirrors of the fiber-tip FPI. Under UV illumination, photo-generated carriers increase the material RI of ZnO and hence the optical path length of the FPI, resulting in a redshift of the interference wavelengths.

The fabrication flowchart of the proposed PD is illustrated in Fig. 1(c). Firstly, a single ZnO micro-pillar on a silicon substrate is transferred to lie in the center of the cleaved end of a SMF with a core/cladding diameter of 8/125 μm by a tungsten probe, which is attached to a computer-controlled micromanipulator with a spatial resolution of 120 nm. The ZnO micro-pillar and the optical fiber tip were directly adsorbed by the Van der Waals force. Note that the preparation method of ZnO micro-pillars can refer to the chemical vapor deposition method reported by Xu et al. [32]. Then the fiber-tip ZnO micro-pillar is coated with Ag-film by direct

Optics EXPRESS

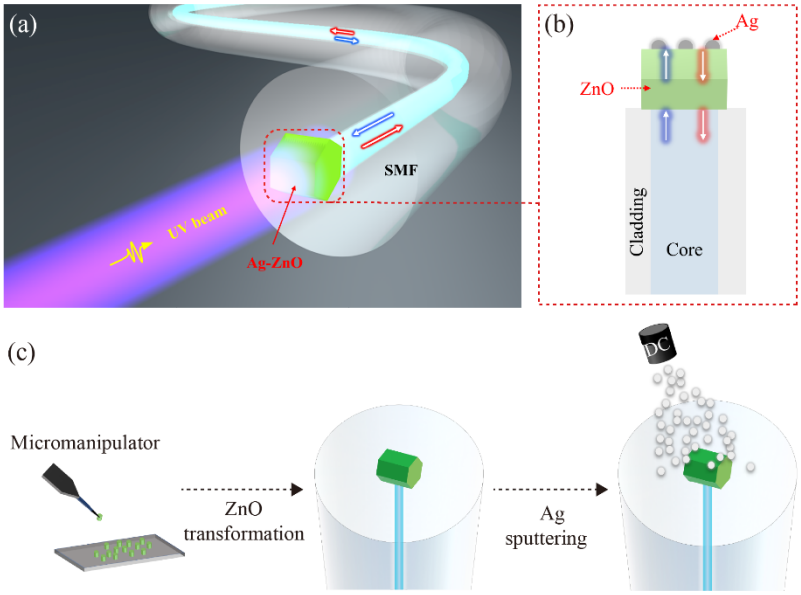

Fig. 1. (a) 3D schematic diagram of the proposed fiber-optic UV PD. (b) 2D magnification of the UV sensing head as shown in (a), where the upper and lower parallel sidewalls of ZnO micro-pillar reflect the detection light delivered through the fiber core, forming a fiber-tip FPI. (c) Fabrication flowchart of the proposed device.

current (DC) magnetron sputtering technique. The sputtering targets is Ag (99.99% purity) disk with a diameter of 2 inches. During deposition the sputtering current is 40 mA and the Argon pressure is kept at 2.0 Pa. The deposition rate is estimated to be 4 nm/s and the film thickness can be controlled by sputtering time. These procedures ensure the simplicity and high repeatability of the device fabrication.

3. Result and discussion

Figure 2(a) shows the crystal structure of pure ZnO micro-pillars, characterized by X-ray diffraction (XRD), which is in consistence with the standard diffraction pattern of ZnO crystal. It indicates that the hexagonal ZnO micro-pillar with high crystallinity has been successfully prepared. After the ZnO micro-pillar is sputtered with Ag for 60 s, electron diffraction X-ray (EDX) spectrum analysis is performed to evident the existence of Ag and the element proportion of the decorated ZnO micro-pillar, as shown in Fig. 2(b). The scanning electron microscope (SEM) images of the proposed device are presented in Fig. 2(c)-(e) with magnification times of 2000, 35000 and 60000, respectively, where a single Ag-decorated ZnO micro-pillar with smooth sidewalls can be seen clearly to be placed on the core region of the SMF fiber end. Moreover, the discontinuous island-like structure of the Ag-film can be observed on the surface of ZnO micro-pillar, which is expected to improve the sensitivity of the fiber-optic UV PD through plasmonic effect. The element distribution and relative proportion of O, Ag and Zn of the abovementioned device can be observed in Fig. 2(f)-(h). It should be noted that Ag element distribution exceeds the ZnO micro-pillar area due to the non-ideal mask used during sputtering coating.

Figure 3 shows the experimental setup for sensitivity test of the proposed fiber-optic UV PD. A femtosecond (fs) laser (Light conversion, PH1) with an output center wavelength of 1026 nm and a repetition rate of 200 kHz is employed to irradiate the device. Pulses generated from the fs

Optics EXPRESS

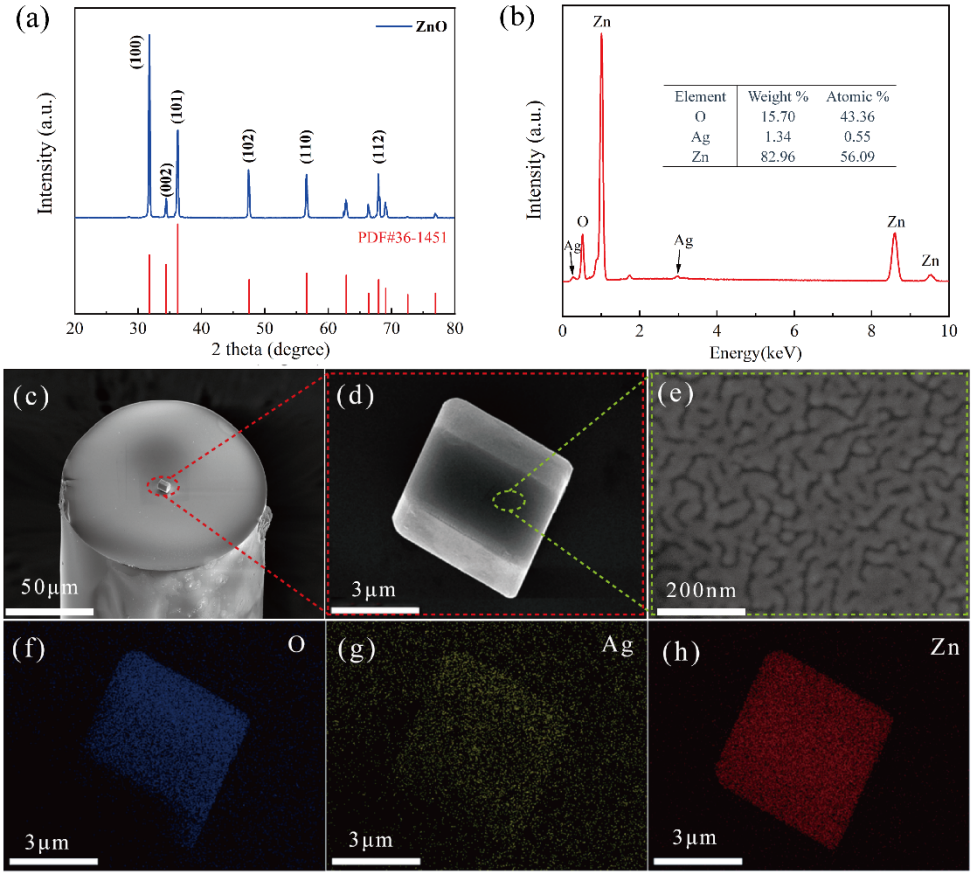

Fig. 2. (a) The XRD pattern of ZnO micro-pillars prepared. (b) The point EDX spectrum of the ZnO micro-pillar after 60 s Ag sputtering. (c)-(e) SEM image of the fiber-optic UV PD with 60 s Ag sputtering in magnification times of 2000, 35000 and 60000, respectively. The light grey island-like structure is Ag and the black stripes correspond to the substrate ZnO in (e). (f)-(h) The EDX elemental mapping images of O, Ag, and Zn, corresponding to (d).

laser are frequency-quadrupled (wavelength λ=257 nm) through an external optical frequency multiplier and then delivered to the Ag-decorated ZnO micro-pillar through a focusing lens. Note that the fs pulses (λ=1026 nm) can also be frequency doubled to λ=513 nm through the same frequency multiplier. The sample is connected to a supercontinuum light source (YSL,SC-5) and an optical spectrum analyzer (Yokogawa, AQ6370B) through an optical fiber circulator to monitor its interference spectrum in real-time.

Under UV illumination, the sample with pristine ZnO micro-pillar exhibits a redshift of interference wavelengths with the increase of light intensity, as depicted in Fig. 4(a). Through lining fitting, the 3.3-nm wavelength shift corresponding to a sensitivity of 0.29 nm/(W·cm^{-2}) can be obtained. When the ZnO micro-pillar is sputtered with Ag for 60 s, the wavelength shift of the device is dramatically raised to 13.4 nm under UV irradiation with an intensity of 11.81 W/cm^2, as plotted in Fig. 4(b), and the sensitivity reaches to 1.13 nm/(W·cm^{-2}). Apparently, the introduction of silver film significantly enhances the device's sensitivity. In order to understand the influence of Ag decoration on the device sensitivity, a series of samples are fabricated with changing the Ag sputtering time from 15 s to 115 s. All the samples are prepared from the same batch of ZnO micro-pillar (similar morphology and element composition) and exhibit nearly the

Optics EXPRESS

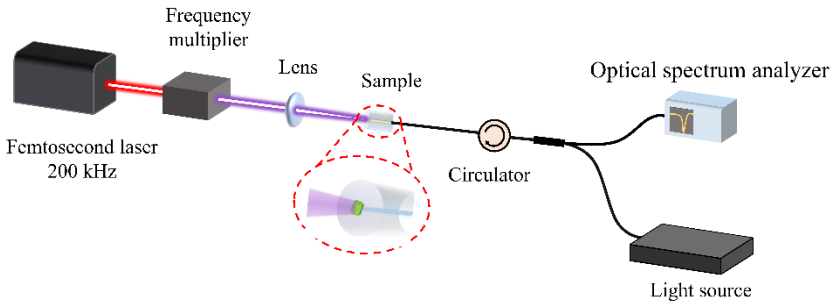

Fig. 3. The experimental setup for sensitivity test of the fiber-optic UV PD.

same sensitivity before Ag sputtering to ensure the accuracy of the experiment. The interference wavelength shift of these samples as a function of light intensity is plotted in Fig. 4(c), where one can see that the device sensitivity has been improved and is closely related to the Ag sputtering time (namely, film thickness). For clarity, enhancement factor is defined here as the sensitivity ratio of Ag-decorated sample to that of the device with pristine ZnO micro-pillar, which is presented in Fig. 4(d) along with the device sensitivity. With sputtering time increasing, the sensitivity and enhancement factor rise first and then decrease, reaching a maximum of 3.9 when the sputtering time is 60 s. This should be closely related to the morphology and distribution of silver film on the surface of ZnO. As shown clearly in Fig. 2(e) above, the thin Ag-film prepared by magnetron sputtering exhibits a discontinuous island-like structure, which is beneficial for the absorption of UV [33]. Moreover, silver can form Schottky contact with the ZnO surface, which leads to a significant widening of the depletion layer and results in a more pronounced change in carrier concentration combined with the plasmonic effect under UV irradiation. On the other hand, a continuous Ag film is easily formed with sputtering time further increased, which will increase the UV reflection, weaken the plasmonic effect, reduce the absorption and thus degrade the sensitivity.

The sample with Ag sputtering time of 60 s is also illuminated by visible (513 nm) and near infrared (1026 nm) laser beam to verify whether the photothermal effect will affect the shift of interference wavelength. Due to the non-absorption of ZnO in these bands, it can be considered that only photothermal effect (consequently induce a temperature variation) dominates the shift of interference wavelength here. As can be seen from Fig. 5, negligible wavelength shift can be found with the light intensity increasing of 513 and 1026 nm laser beam. For comparison, the results of samples with pristine and Ag-decorated ZnO micro-pillar under the illumination of 257 nm laser beam are also presented in Fig. 5. Therefore, the influence of temperature variation during light absorption on the UV sensitivity of the proposed device can be ignored.

Response time is an important indicator for evaluating the performance of PDs. A Nd:YAG laser (Quanta-ray, Lab-170-10) that outputs laser pulses with a frequency-quadrupled wavelength of 266 nm, a repetition rate of 10 Hz and a pulse duration of 5 ns is employed to excite the sample. A lens is used to focus the UV laser beam onto the sample surface. To trace and record the temporal response, the fiber pigtail of the sample is connected to a tunable laser (Agilent Technologies, Model 81940A) and a commercial available PD (New Focus, Model 2053) through a fiber circulator, and the wavelength shift of the sample is converted into an intensity fluctuation of the monitoring laser beam that can be recorded by the abovementioned PD and an oscilloscope (Tektronix, MDO 3054), which can refer to the edge filter method [34].

Figure 6(a) shows the temporal response of the sample under the excitation of 10 consecutive laser pulses, where it can be seen that the device exhibits fast response and good stability. With the definition of rise and fall time to be the time taken by the signal to change from 10% to 90%

Optics EXPRESS

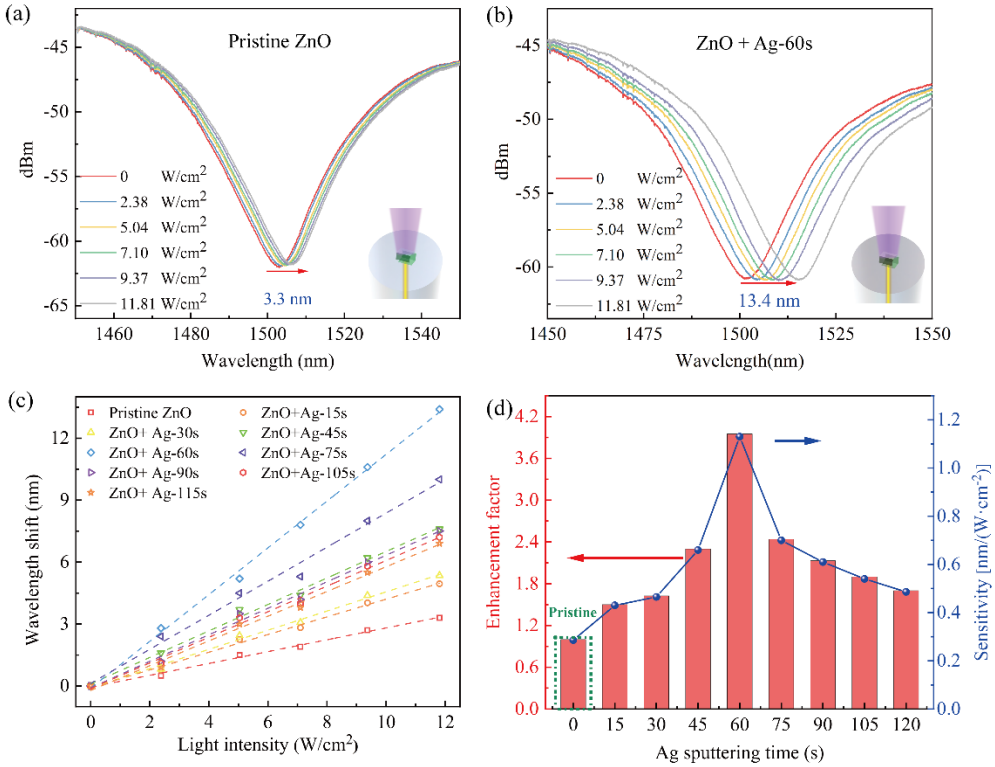

Fig. 4. (a) and (b) The interference spectrum evolution of the fiber-optic UV PD under 257-nm laser irradiation with pristine and Ag-decorated (sputtering time 60 s) ZnO micro-pillar. (c) Wavelength shift as a function of UV light intensity for Ag-decorated samples with different sputtering time. (d) Sensitivity and enhancement factor as a function of sputtering time.

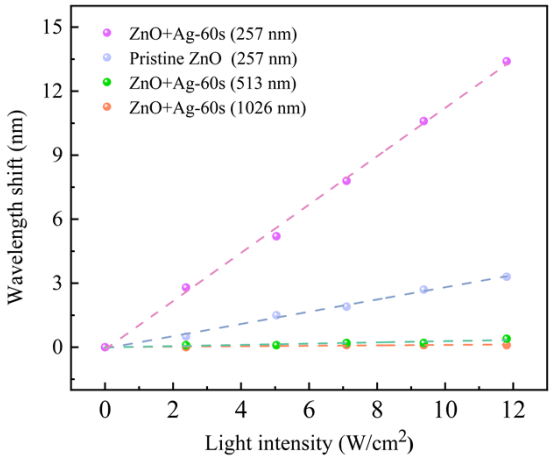

Fig. 5. Wavelength response of the proposed fiber-optic UV PD.

Optics EXPRESS

between its low level to the high level and vice versa, the rise and fall time can be calculated to be 35 ns and 40 µs, respectively, according to the rising and falling edges of a single period of temporal response, as shown in Fig. 6(b). The proposed device exhibits faster response compared to that of the previously reported UV PDs, as listed in Table 1. This is mainly because the response speed of the device only depends on the speed of carrier generation in the bulk of ZnO. Meanwhile, the small volume of ZnO micro-pillar may weaken the carrier diffusion and thus improve the temporal response of the device. On the other hand, the slow decay time may be mainly caused by ultra-long lifetime of the trapped states, which may come from defects in ZnO, or surface damage during device processing. In addition, oxygen adsorption on the ZnO surface and grain boundaries may also deteriorate the decay time [35,36].

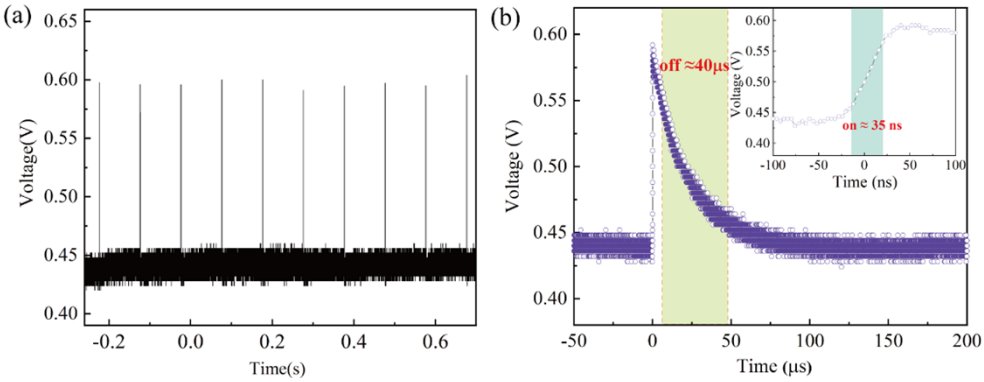

Fig. 6. (a) Temporal response of the fiber-optic UV PD under the excitation of 10-Hz 266-nm pulsed laser irradiation with an intensity of 7.01 W/cm^2. (b) Magnification of a single period of temporal response. Inset: rising edge of the response.

Table 1. A comparison of ultraviolet photodetectors fabricated using various materials

UV PD	λ	Pulse duration	Responsivity/ Sensitivity	t_{rise}	t_{fall}	Ref
ZnO nanowire	266 nm	——	1.657 nm/(W·cm^{-2})	0.43 ms	0.47 ms	[28]
ZnO nanowire	266 nm	——	0.288 nm/(W·cm^{-2})	0.56 ms	0.7 ms	[29]
Se/ZnO	370 nm	3-5 ns	2.65 mA W^{-1}	0.69 ms	13.5 ms	[37]
$BaTiO_3$/ZnO	355 nm	3-5 ns	1.28 mA W^{-1}	0.11 ms	5.08 ms	[38]
Se/n-Si	355 nm	3-5 ns	——	235 µs	1.74 ms	[39]
Se/TiO_2 nanotubes	355 nm	3-5 ns	——	1.4 ms	7.4 ms	[40]
ZnO /CuSCN	355 nm	5 ns	9.5 A W^{-1}	500 ns	6.7 µs	[41]
GaN/MoO_{3-x} nanorod	355 nm	——	160 A W^{-1}	127 ns	345 µs	[42]
CuZnS/GaN	355 nm	3-5 ns	0.36 A W^{-1}	0.14 ms	40 ms	[43]
ZnO/Ag	257nm	5 ns	1.13 nm/(W·cm^{-2})	35 ns	40 µs	This work

The sensing mechanism of the proposed device is mainly depends on the material RI change that caused by the carrier generation during UV irradiation of ZnO micro-pillar. The increase of material RI will lengthening the optical path of the ZnO FPI, thus resulting in the redshift of the interference wavelengths. As well known, large changes of the absorption coefficient can be caused by the existed carriers in semiconductors through the competitive energy band filling effect and bandgap shrinkage effect, which can produce a considerable RI change in

Optics EXPRESS

semiconductors [44] according to the Kramers–Kronig relationship [45],

$$\Delta n\,(N,P,E) = \frac{2c\hbar}{e^2} P \int_0^\infty \frac{\Delta\alpha\,(N,P,E')}{E'^2 - E^2} dE' \tag{1}$$

where c is the speed of light, $\hbar$ is Planck's constant, e is the electron charge, E is the photon energy, and $P\int$ indicates the principal value of the integral. The term $\Delta\alpha$ represents the change of material absorption coefficient, N and P are the concentrations of free electrons and holes, respectively. In the case of relatively high photocarrier concentration, the absorption coefficient of ZnO will be increased due to the bandgap shrinkage effect [46], which results in a measurable RI increase and has been explained exclusively elsewhere.

For the proposed device, the modification of silver plays an important role for the sensitivity enhancement, or namely the RI variation of ZnO is significantly improved by the modification of silver, which is closely related to the thickness change of the surface depletion layer in ZnO [21]. Specifically, the surface of pure ZnO micro-pillar becomes highly active due to the adsorption of oxygen. Affected by the surface states and defect energy levels, oxygen will capture electrons from the surface layer of ZnO, forming a depletion layer with a certain thickness on the surface of ZnO [$O_{2(g)} + e^- \rightarrow O^-_{2(ad)}$], as shown in Fig. 7(a). When irradiated with UV, a large number of free electrons and holes are created inside the ZnO [$E = h\upsilon \rightarrow e^- + h^+$]. At the same time, the electrons captured by oxygen are released to the surface area of ZnO again and the thickness of the depletion layer decreases [$h^+ + O^-_{2(ad)} = O_{2(g)}$], as illustrated in Fig. 7(c). Proportionately, the thickness of the surface depletion layer will exhibit more obvious changes for Ag-decorated ZnO micro-pillars, as demonstrated in Fig. 7(b) and 7(d). Due to catalytic action of Ag, the deposition of silver will increase the adsorption of oxygen on ZnO, so that more electrons gather on the surface of ZnO compared to that of the pristine ZnO [47,48]. The local Schottky barrier at the interface between silver and ZnO will increase the thickness of depletion region and the surface electric field, resulting in a significantly expanded surface depletion layer and a smaller carrier density in the ZnO micro-pillar [21,49]. Similarly, under UV illumination, the depletion layer

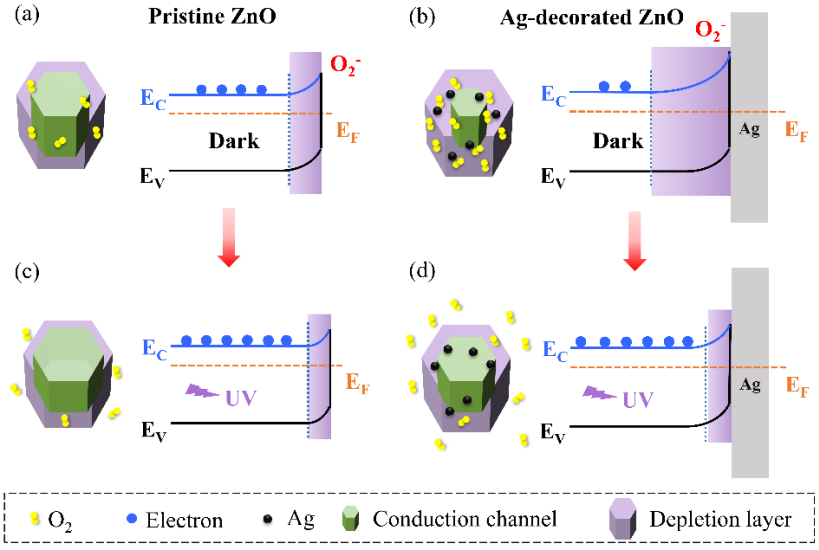

Fig. 7. Illustration of UV sensing mechanism of a single ZnO micro-pillar and Ag-decorated ZnO micro-pillar based on ion sorption model and energy band diagram. Pristine ZnO micro-pillar in dark (a) and under UV illumination (c); Ag-decorated ZnO micro-pillar in dark (b) and under UV illumination (d).

Optics EXPRESS

significantly shrinks under the synergistic effect of large amounts of photo-generated carriers and the released electrons that initially captured by oxygen. Compared to that of the pristine ZnO micro-pillar, the variation in the thickness of surface depletion layer is more obvious under UV irradiation, and the unpaired electrons in the non-depletion layer will significantly promote the increase of carrier concentration in the material. Hence, Ag-decorated ZnO micro-pillar exhibits a more obvious change in RI compared to that of the pristine ones. Moreover, the potential plasmonic effect may also significantly improve the charge carrier generation and transportation due to the existence of island-like Ag [50,51], which is beneficial to improve the response speed of the device.

4. Conclusion

In summary, we have demonstrated an ultra-compact and fast-response fiber-optic UV PD by integrating a ZnO micro-pillar with an optical fiber. The semiconductor micro-pillar acts as a Fabry-Pérot interferometer, of which the optical path is lengthened and the interference wavelengths redshift under UV illumination through the photo-carrier induced RI change. This phenomenon can be enhanced by coating a discontinuous Ag-film with an island-like structure onto the surface of ZnO micro-pillars. The proposed device exhibits a UV sensitivity of up to 1.13 nm/(W·cm^{-2}), which is about 4 times compared to that of using a pristine ZnO micro-pillar. The fiber-optic UV PD also shows very fast response with a rise time of 35 ns and a decay time of 40 µs. The proposed device dispenses with complex circuit structure and employs an all-optical detection scheme. The fabrication procedure offers a simple, low cost and highly repeatable method of manufacturing fast-response UV PDs. The demonstrated device exhibits compactness, flexibility, fast response and immune to electromagnetic interference, which may pave a new way for the next generation of photodetection devices.

Funding. Science and Technology Innovation Commission of Shenzhen (JCYJ20200109114001806, JCYJ20220818095615034); National Natural Science Foundation of China (62122057, 91860138).

Disclosures. The authors declare no conflicts of interest.

Data availability. Data underlying the results presented in this paper are not publicly available at this time but may be obtained from the authors upon reasonable request.

References

1. S. Knobelspies, A. Daus, G. Cantarella, L. Petti, N. Münzenrieder, G. Tröster, and G. A. Salvatore, "Flexible a-IGZO Phototransistor for Instantaneous and Cumulative UV-Exposure Monitoring for Skin Health," Adv. Electron. Mater. **2**(10), 1600273 (2016).
2. E. Munoz, E. Monroy, J. Pau, F. Calle, F. Omnes, and P. Gibart, "III nitrides and UV detection," J. Phys.: Condens. Matter **13**(32), 7115 (2001).
3. H. Fang, C. Zheng, L. Wu, Y. Li, J. Cai, M. Hu, X. Fang, R. Ma, Q. Wang, and H. Wang, "Solution-processed self-powered transparent ultraviolet photodetectors with ultrafast response speed for high-performance communication system," Adv. Funct. Mater. **29**(20), 1809013 (2019).
4. M. C. Traub, W. Longsine, and V. N. Truskett, "Advances in nanoimprint lithography," Annu. Rev. Chem. Biomol. Eng. **7**(1), 583–604 (2016).
5. H. Chen, K. Liu, L. Hu, A. A. Al-Ghamdi, and X. Fang, "New concept ultraviolet photodetectors," Mater. Today (Oxford, U. K.) **18**(9), 493–502 (2015).
6. F. Guo, B. Yang, Y. Yuan, Z. Xiao, Q. Dong, Y. Bi, and J. Huang, "A nanocomposite ultraviolet photodetector based on interfacial trap-controlled charge injection," Nat. Nanotechnol. **7**(12), 798–802 (2012).
7. L. Jia, W. Zheng, and F. Huang, "Vacuum-ultraviolet photodetectors," PhotoniX **1**(1), 22–25 (2020).
8. J. Chen, W. Ouyang, W. Yang, J. H. He, and X. Fang, "Recent progress of heterojunction ultraviolet photodetectors: materials, integrations, and applications," Adv. Funct. Mater. **30**(16), 1909909 (2020).
9. L. Peng, L. Hu, and X. Fang, "Low-dimensional nanostructure ultraviolet photodetectors," Adv. Mater. **25**(37), 5321–5328 (2013).
10. W. Tian, H. Lu, and L. Li, "Nanoscale ultraviolet photodetectors based on onedimensional metal oxide nanostructures," Nano Res. **8**(2), 382–405 (2015).
11. Ü. Özgür, Y. I. Alivov, C. Liu, A. Teke, M. A. Reshchikov, S. Doğan, V. Avrutin, S. J. Cho, and H. Morkoç, "A comprehensive review of ZnO materials and devices," J. Appl. Phys. (Melville, NY, U. S.) **98**(4), 041301 (2005).
12. K. Liu, M. Sakurai, and M. Aono, "ZnO-based ultraviolet photodetectors," Sensors **10**(9), 8604–8634 (2010).

Optics EXPRESS

13. L. Schmidt-Mende and J. L. MacManus-Driscoll, "ZnO-nanostructures, defects, and devices," Mater. Today (Oxford, U. K.) **10**(5), 40–48 (2007).
14. R. Valiev, "Nanomaterial advantage," Nature **419**(6910), 887–889 (2002).
15. H. Kind, H. Yan, B. Messer, M. Law, and P. Yang, "Nanowire ultraviolet photodetectors and optical switches," Adv. Mater. **14**(2), 158–160 (2002).
16. H. K. Yadav, K. Sreenivas, and V. Gupta, "Enhanced response from metal/ZnO bilayer ultraviolet photodetector," Appl. Phys. Lett. **90**(17), 172113 (2007).
17. S. Liang, H. Sheng, Y. Liu, Z. Huo, Y. Lu, and H. Shen, "ZnO Schottky ultraviolet photodetectors," J. Cryst. Growth **225**(2-4), 110–113 (2001).
18. C. L. Hsu and S. J. Chang, "Doped ZnO 1D nanostructures: synthesis, properties, and photodetector application," Small **10**(22), 4562–4585 (2014).
19. F. Yang, M. Zheng, L. Zhao, J. Guo, B. Zhang, G. Gu, G. Cheng, and Z. Du, "The high-speed ultraviolet photodetector of ZnO nanowire Schottky barrier based on the triboelectric-nanogenerator-powered surface-ionic-gate," Nano Energy **60**, 680–688 (2019).
20. J. Huang, Q. Li, X. Lu, J. Meng, and Z. Li, "LSPR-Enhanced Pyro-Phototronic Effect for UV Detection with an Ag-ZnO Schottky Junction Device," Adv. Mater. Interfaces **9**(23), 2200327 (2022).
21. O. Lupan, V. Cretu, V. Postica, M. Ahmadi, B. R. Cuenya, L. Chow, I. Tiginyanu, B. Viana, T. Pauporté, and R. Adelung, "Silver-doped zinc oxide single nanowire multifunctional nanosensor with a significant enhancement in response," Sens. Actuators, B **223**, 893–903 (2016).
22. X. Zhao, F. Wang, L. Shi, Y. Wang, H. Zhao, and D. Zhao, "Performance enhancement in ZnO nanowire based double Schottky-barrier photodetector by applying optimized Ag nanoparticles," RSC Adv. **6**(6), 4634–4639 (2016).
23. D. Lin, H. Wu, W. Zhang, H. Li, and W. Pan, "Enhanced UV photoresponse from heterostructured Ag–ZnO nanowires," Appl. Phys. Lett. **94**(17), 172103 (2009).
24. Y. Zou, Y. Zhang, Y. Hu, and H. Gu, "Ultraviolet Detectors Based on Wide Bandgap Semiconductor Nanowire: A Review," Sensors **18**(7), 2072 (2018).
25. T. Zhai, X. Fang, M. Liao, X. Xu, H. Zeng, B. Yoshio, and D. Golberg, "A comprehensive review of one-dimensional metal-oxide nanostructure photodetectors," Sensors **9**(8), 6504–6529 (2009).
26. Y. Wang, L. Zhu, Y. Feng, Z. Wang, and Z. L. Wang, "Comprehensive Pyro-Phototronic Effect Enhanced Ultraviolet Detector with ZnO/Ag Schottky Junction," Adv. Funct. Mater. **29**(5), 1807111 (2019).
27. N. Nasiri, D. Jin, and A. Tricoli, "Nanoarchitechtonics of Visible-Blind Ultraviolet Photodetector Materials: Critical Features and Nano-Microfabrication," Adv. Opt. Mater. **7**(2), 1800580 (2019).
28. L. Zhang, Y. Wang, H. Wu, M. Hou, J. Wang, L. Zhang, C. Liao, S. Liu, and Y. Wang, "A ZnO nanowire-based microfiber coupler for all-optical photodetection applications," Nanoscale **11**(17), 8319–8326 (2019).
29. H. Wu, Y. Wang, L. Zhang, K. Guo, Y. Huang, C. Liao, and Y. Wang, "ZnO Microwire-Based Fiber-Tip Fabry-Pérot Interferometer for Deep Ultraviolet Sensing," J. Lightwave Technol. **39**(12), 4225–4229 (2021).
30. Y.-F. Xiong, J.-H. Chen, Y.-Q. Lu, and F. Xu, "Broadband Optical-Fiber-Compatible Photodetector Based on a Graphene-MoS_2-WS_2 Heterostructure with a Synergetic Photogenerating Mechanism," Adv. Electron. Mater. **5**(1), 1800562 (2019).
31. Y. Xiong, H. Xu, Y. Wang, C. Wu, Z. Ding, M. Chen, Y. Hao, Y. Chen, and F. Xu, "Ultracompact Multicore Fiber De-Multiplexer Using an Endface-Integrating Graphene Photodetector Array," ACS Photonics **9**(5), 1808–1813 (2022).
32. C. X. Xu, X. W. Sun, Z. L. Dong, and M. B. Yu, "Zinc oxide nanodisk," Appl. Phys. Lett. **85**(17), 3878–3880 (2004).
33. X. Wang, K. Liu, X. Chen, B. Li, M. Jiang, Z. Zhang, H. Zhao, and D. Shen, "Highly Wavelength-Selective Enhancement of Responsivity in Ag Nanoparticle-Modified ZnO UV Photodetector," ACS Appl. Mater. Interfaces **9**(6), 5574–5579 (2017).
34. C. Liao, D. N. Wang, Y. Li, T. Sun, and K. T. Grattan, "Temporal thermal response of Type II-IR fiber Bragg gratings," Appl. Opt. **48**(16), 3001–3007 (2009).
35. Y. Liu, C. Gorla, S. Liang, N. Emanetoglu, Y. Lu, H. Shen, and M. Wraback, "Ultraviolet detectors based on epitaxial ZnO films grown by MOCVD," J. Electron. Mater. **29**(1), 69–74 (2000).
36. M. Mamat, M. Sahdan, S. Amizam, H. Rafaie, Z. Khusaimi, and M. Rusop, "Al Doped ZnO Thin Film Based Ultraviolet Photo-Conductive Sensor Prepared by Sol-Gel Spin-Coating Method," in *AIP Conference Proceedings*, (American Institute of Physics, 2009), pp. 591–595.
37. K. Hu, F. Teng, L. Zheng, P. Yu, Z. Zhang, H. Chen, and X. Fang, "Binary response Se/ZnO p-n heterojunction UV photodetector with high on/off ratio and fast speed," Laser Photonics Rev. **11**(1), 1600257 (2017).
38. Y. Zhang, X. Zhao, J. Chen, S. Li, W. Yang, and X. Fang, "Self-Polarized $BaTiO_3$ for Greatly Enhanced Performance of ZnO UV Photodetector by Regulating the Distribution of Electron Concentration," Adv. Funct. Mater. **30**(5), 1907650 (2020).
39. W. Yang, K. Hu, F. Teng, J. Weng, Y. Zhang, and X. Fang, "High-Performance Silicon-Compatible Large-Area UV-to-Visible Broadband Photodetector Based on Integrated Lattice-Matched Type II Se/n-Si Heterojunctions," Nano Lett. **18**(8), 4697–4703 (2018).
40. L. Zheng, K. Hu, F. Teng, and X. Fang, "Novel UV-Visible Photodetector in Photovoltaic Mode with Fast Response and Ultrahigh Photosensitivity Employing Se/TiO_2 Nanotubes Heterojunction," Small **13**(5), 1602448 (2017).

Optics EXPRESS

41. S. M. Hatch, J. Briscoe, and S. Dunn, "A self-powered ZnO-nanorod/CuSCN UV photodetector exhibiting rapid response," Adv. Mater. **25**(6), 867–871 (2013).
42. Y. Zheng, Y. Li, X. Tang, W. Wang, and G. Li, "A Self-Powered High-Performance UV Photodetector Based on Core-Shell GaN/MoO_{3-x} Nanorod Array Heterojunction," Adv. Opt. Mater. **8**(15), 2000197 (2020).
43. Y. Zhang and W. Song, "High performance self-powered CuZnS/GaN UV photodetectors with ultrahigh on/off ratio (3×10^8)," J. Mater. Chem. C **9**(14), 4799–4807 (2021).
44. T. Shen, J. Wang, Z. Xia, X. Dai, B. Li, and Y. Feng, "Ultraviolet sensing characteristics of Ag-doped ZnO micro-nano fiber," Sens. Actuators, A **307**, 111989 (2020).
45. V. Lucarini, J. J. Saarinen, K.-E. Peiponen, and E. M. Vartiainen, *Kramers-Kronig relations in optical materials research* (Springer Science & Business Media, 2005).
46. A. P. Roth, J. B. Webb, and D. F. Williams, "Band-gap narrowing in heavily defect-doped ZnO," Phys. Rev. B **25**(12), 7836–7839 (1982).
47. W. Xie, Y. Li, W. Sun, J. Huang, H. Xie, and X. Zhao, "Surface modification of ZnO with Ag improves its photocatalytic efficiency and photostability," J. Photochem. Photobiol., A **216**(2-3), 149–155 (2010).
48. Y. Zheng, L. Zheng, Y. Zhan, X. Lin, Q. Zheng, and K. Wei, "Ag/ZnO heterostructure nanocrystals: synthesis, characterization, and photocatalysis," Inorg. Chem. **46**(17), 6980–6986 (2007).
49. Z. S. Hosseini, H. A. Bafrani, A. Naseri, and A. Z. Moshfegh, "High-performance UV-Vis-NIR photodetectors based on plasmonic effect in Au nanoparticles/ZnO nanofibers," Appl. Surf. Sci. **483**, 1110–1117 (2019).
50. W.-H. Lin, Y.-H. Chiu, P.-W. Shao, and Y.-J. Hsu, "Metal-particle-decorated ZnO nanocrystals: photocatalysis and charge dynamics," ACS Appl. Mater. Interfaces **8**(48), 32754–32763 (2016).
51. H. Ding, J. Shao, Y. Ding, W. Liu, H. Tian, and X. Li, "One-dimensional Au–ZnO heteronanostructures for ultraviolet light detectors by a two-step dielectrophoretic assembly method," ACS Appl. Mater. Interfaces **7**(23), 12713–12718 (2015).